AGU100 ADVANCING EARTH AND SPACE SCIENCE

Geophysical Research Letters

RESEARCH LETTER
10.1029/2018GL078495

Special Section:
Bridging Weather and Climate: Subseasonal-to-Seasonal (S2S) Prediction

Key Points:
- The variance of 20–30 day periodicity of precipitation and eddy kinetic energy in austral summer is projected to intensify by 20% by the 2070s
- The projected increase of intraseasonal variability in precipitation and eddy kinetic energy is larger than the change of seasonal mean
- While weak in current climate, the 20–30 day periodicity of precipitation and EKE in austral winter becomes prominent as climate warms

Supporting Information:
- Supporting Information S1

Correspondence to:
L. Wang,
leiwang@fas.harvard.edu

Citation:
Wang, L., Lu, J., & Kuang, Z. (2018). A robust increase of the intraseasonal periodic behavior of the precipitation and Eddy kinetic energy in a warming climate. *Geophysical Research Letters*, *45*. https://doi.org/10.1029/2018GL078495

Received 25 APR 2018
Accepted 30 MAY 2018
Accepted article online 5 JUN 2018

A Robust Increase of the Intraseasonal Periodic Behavior of the Precipitation and Eddy Kinetic Energy in a Warming Climate

Lei Wang[1,2], Jian Lu[3], and Zhiming Kuang[1,2]

[1]Harvard University, Department of Earth and Planetary Sciences, Cambridge, MA, USA, [2]Harvard University, John A. Paulson School of Engineering and Applied Sciences, Cambridge, MA, USA, [3]Pacific Northwest National Laboratory, Atmospheric Sciences and Global Change Division, Richland, WA, USA

Abstract Precipitation and storm track activity in the Southern Hemisphere feature a remarkable 20 to 30-day periodicity known as baroclinic annular mode. In climate model projections following the representative concentration pathway 8.5 scenario, this work finds a robust increase of intraseasonal variability of the precipitation and density-weighted eddy kinetic energy at the 20–30 day frequency range by 25% and 20%, respectively, in austral summer toward the end of the century, despite small changes in seasonal-mean quantities at corresponding latitudes. These results suggest that a warming climate can feature a stronger dynamical organization of the 20–30 day periodicity by the moist baroclinic waves. For austral winter, the weak 20–30 day periodicity in the current climate becomes a prominent mode of quasiperiodic variability toward the end of the century in these model projections. This work identifies both the increase of diabatic heating and the enhancements of the waveguide effects as candidate mechanisms.

Plain Language Summary This work reports a robust increase of the intraseasonal periodic behavior in the Southern Hemisphere storm track with important implications on midlatitude hydrological extremes. While it is well-documented that the jet stream will shift poleward in a warming climate, this is the first contribution that identifies how the intraseasonal variability of the storm tracks would change in response to global warming in comprehensive climate models (National Center for Atmospheric Research Large Ensemble project and CMIP5 outputs). Evidence suggests that both the increase of moisture and the change of a climatological basic state can contribute to the intensification of the intraseasonal variability, which implies a more predictable baroclinic annular mode in the Southern Hemisphere in a warmer climate. This finding serves as a stimulus for future studies to unveil the role of changing diabatic heating on the intraseasonal variability in the midlatitudes.

1. Introduction

A recent series of work have revealed a dominant mode of variability that has a clear periodicity centered at 25 days known as baroclinic annular mode (BAM; Thompson & Barnes, 2014; Thompson & Woodworth, 2014; Wang & Nakamura, 2015, 2016; Zurita-Gotor, 2017). Similar to the Madden-Julian Oscillation in the tropics, this 20–30 day periodicity in the midlatitudes might be the single most important oscillatory signal in the midlatitudes with the potential for advancing subseasonal to seasonal prediction. As discussed in Wang and Nakamura (2016), the annularity in the Southern Hemisphere (SH) circulation affords the possibility that winds, after blowing over the entire latitudinal circle, are able to reenter the domain. This provides a waveguide effect for synoptic Rossby waves of similar horizontal and vertical structures to constructively and destructively interfere with each other, creating an overall amplitude modulation of its wave packet on a time scale of 20–30 day.

Synoptic waves and zonal-mean zonal flow are strongly coupled; hence, a deep understanding of the change of the 20–30 day periodicity in the wave processes must rely on and should be consistent with the change of the zonal-mean circulation. The most significant response of the midlatitude zonal-mean circulation to a warmer climate is a poleward shift in jet streams (Barnes & Polvani, 2013; Chang et al., 2012; Grise & Polvani, 2014; Hall et al., 1994; Yin, 2005), and a major part of this change is realized through an enhanced irreversible mixing of potential vorticity (PV) during Rossby waves breaking on the flanks of the jet (Lee & Feldstein, 2013; Lu et al., 2014; Nie et al., 2015; Wang & Lee, 2016). Therefore, as an agent modulating the jet stream, the transient eddies play an indispensable role in setting up the midlatitude circulation response. In typical lifecycles, eddies initially grow from surface thermal perturbations and subsequently get mutually reinforced with the upper tropospheric PV perturbations. The issue of the jet shift pertains to the later stage of life cycles when transient eddies deposit eddy kinetic energy (EKE) to the zonal-mean flow, whereas it remains unclear how BAM, which is more pertinent to the growth amplitude of the baroclinic eddies, would respond to climate warming. In particular, how will the midlatitude wave activity, especially its 20–30 day periodicity—the BAM, respond to increasing greenhouse gas forcing and the corresponding increase of moisture, as well as a more poleward shifted jet?

While the fundamental nature of the 20–30 day periodicity may have its root in dry dynamics, as it can be identified from idealized dry two-layer quasi-geostrophic models (Wang, 2016), diabatic processes, such as the latent heating from water vapor condensation, through their significant effect on the evolution of Rossby waves (Ahmadi-Givi et al., 2004; Hoskins et al., 1985), have the potential to regulate the intensity of the 20–30 day periodic behavior. In a warming climate, the SH storm track intensifies with an increased mean available potential energy of the atmosphere (O'Gorman, 2010) and the baroclinic eddies are energized with enhanced diabatic heating (Tamarin-Brodsky & Kaspi, 2017). With the increasing specific humidity in the atmosphere in a warming climate, the conversion rate from eddy available potential energy to EKE is increasing in the recent decades (Pan et al., 2017), suggesting that the EKE in the troposphere will be more efficiently fueled by the diabatic processes. However, it remains unclear how the intraseasonal variability of baroclinic eddies would change in response to the enhancement of diabatic heating in a warming climate.

The changing intraseasonal variability is essential not only for storm track dynamics but also for the hydrologic cycle's response to a warming climate, as intense precipitation events are modulated intrinsically by large-scale Rossby waves. It has been well recognized in GCM simulations of a warming climate that the change of seasonal-mean precipitation in the subtropical and higher latitudes follows a "dry-get-dryer" and "wet-get-wetter" pattern (Held & Soden, 2006), which leaves the region sandwiched in between—the equatorward side of the midlatitudes where the 20–30 day periodicity primarily occurs—with only a minor change in the seasonal-mean precipitation. Given the small change in the seasonal-mean precipitation, should we expect a similarly small change in the intraseasonal variability of the precipitation? In general, the second moment response (e.g., standard deviation or variance) of internal dynamics is assumed to not change in a warming climate (Thompson et al., 2015). But extreme precipitation is known to increase more rapidly than the mean precipitation due to the thermodynamic effect of the Clausius-Clapeyron relation (O'Gorman & Schneider, 2009), increase of convective available potential energy (Singh et al., 2017), and an increase in the skewness in the vertical motion (Pendergrass & Gerber, 2016). This motivates us to examine the change of the standard deviation of precipitation on intraseasonal time scales—a second moment of precipitation—and its role in the BAM response to climate warming.

2. Materials and Methods

2.1. AMSR-E

The rain rate in the midlatitudes is strongly tied to the storm track activity. With the ability to penetrate through the atmospheric column, microwave radiometers measure precipitation with adequate accuracy and are especially capable of providing almost continuous all-weather observations. We analyze the microwave radiometer-measured precipitation AMSR-E for the period of 2001–2011 (Wentz et al., 2014). After removing the seasonal cycle, we calculate the power spectra of 120-day chunks for each season in each year, where austral summer is defined as December–March and austral winter as June–September. We then average the results among all years.

2.2. Large Ensemble Community Project

We analyze the outputs from the 40-member ensemble of the Community Earth System Model version 1 (CESM1) as part of the Large Ensemble Community Project (LENS; Kay et al., 2015). CESM1 is a fully coupled, global climate model that provides state-of-the-art computer simulations of Earth's climate and contains a Community Atmosphere Model version 5.2 as its atmospheric component with the nominal 1° latitude-longitude resolution. The historical period is defined as 1976–2005 (denoted as HIST), and the RCP 8.5 period is defined as 2071–2100 (denoted as RCP 8.5). With 40 ensemble members, the average is sufficiently representative. At each latitude, the column-averaged EKE is calculated based on a density weighted vertical

10.1029/2018GL078495

integral of the zonal-mean EKE ($\overline{u'^2 + v'^2}$) from ground up to 20 km normalized by the mass within that layer. After being computed individually for each year and each ensemble member, the spectra are then averaged over all available years and ensemble members. Unlike other variables analyzed in this work, the column EKE is calculated from the available daily data from 1996 to 2005 and 2071 to 2080. Given the relatively linear change in the RCP 8.5 scenario, the fractional change of density-weighted EKE is scaled with a factor of 95/75 to be consistently compared with other variables, while still making full use of other variables' 30-year data in the HIST and RCP 8.5 periods, respectively. The ability for calculating interior EKE intraseasonal variability from daily resolution and with full 30 vertical levels is a major strength of the LENS data sets over Coupled Model Inter-comparison Project Phase 5 (CMIP5) data sets, especially valuable for accounting for a significant change of the vertical structure of the EKE intraseasonal variability (see Figure S1). For a check of consistency, we qualitatively reproduced our results in the CMIP5 data sets and identified a consistent change of the intraseasonal variability (see the supporting materials Figures S4–S7).

3. Results

3.1. A Seasonality of the 20–30 Day Periodicity in Precipitation in AMSR-E

The 20–30 day periodicity in the SH storm track is a large-scale mode of variability defined as the leading empirical orthogonal function mode of zonal-mean EKE (Thompson & Woodworth, 2014). Yet a robust BAM can be identified from raw data without empirical orthogonal function filtering or other statistical manipulation (Wang & Nakamura, 2016). Therefore, in this work, we examine the strength of the periodicity based on the latitude-by-latitude raw data.

We start the discussion by showing the power spectra of zonal-mean precipitation in satellite observations. In Figure 1, AMSR-E rain rate demonstrates a clear peak around 20–30 days around 46°S in the austral summer. The peak latitude is consistent with that of finite-amplitude wave activity (FAWA) and EKE in reanalysis products (Wang & Nakamura, 2016). Nevertheless, unlike EKE or FAWA, the peak of 20–30 day periodicity in precipitation spreads over a wide range of latitudes toward subtropical jet. While the amplitude of baroclinic eddies gradually decay from the peak latitude around 46°S, with an increasing background moisture toward equator, lower latitudes can still exhibit a robust periodicity in the precipitation. Since precipitation reflects diabatic heating due to condensation, this suggests diabatic effects co-vary with the large-scale Rossby waves on the 20–30 day frequency range.

The seasonality of the 20–30 day periodicity in the precipitation is also consistent with that in the EKE or FAWA (Wang & Nakamura, 2016). In austral winter, the intraseasonal variability of rain rate in the SH storm track is substantially weaker, and its peak latitudes are mostly confined to the equatorward of 40°S. The latitude 40°S is near the edge of subtropical jet, where breaking Rossby waves transport a significant amount of moisture into middle-to-high latitudes. This also co-locates with the latitude band of intense atmospheric rivers—long and narrow filaments of large integrated water vapor transport (see the spatial distribution in Guan & Waliser, 2017). While the definition of atmospheric river depends on the threshold chosen, it is conceivable that the 20–30 day periodicity of the precipitation may have a modulating effect on atmospheric rivers; thus, the BAM provides a useful framework for understanding both the internal variation and the future change of atmospheric rivers and the associated precipitation extremes.

3.2. A Robust Increase of Precipitation Variability in CESM Large Ensemble

In Figures 1b and 1f, the CESM ensemble-mean of the historical period (1976–2005) reproduces the observed 20–30 day periodicity in zonal-mean precipitation reasonably well especially for summer, although it still underestimates the observed amplitude of the variance. This underestimation is important to note, and we speculate that it may arise from the coarse model resolution and insufficient representation of the moist processes (such as mesoscale convective systems) in the midlatitudes, although a detailed analysis of the cause of this underestimation is beyond the scope of this study. Further, the details of the spectral shape deviate substantially from that in AMSR-E. Nevertheless, the qualitative features of the 20–30 periodic behavior including the spectral peak frequency, peak latitudes, and its seasonality can be captured in a typical climate model such as the CESM1. Since the CESM1 model can simulate a reasonable BAM including its signatures in the hydrological cycle, we now evaluate its change in a warming climate.

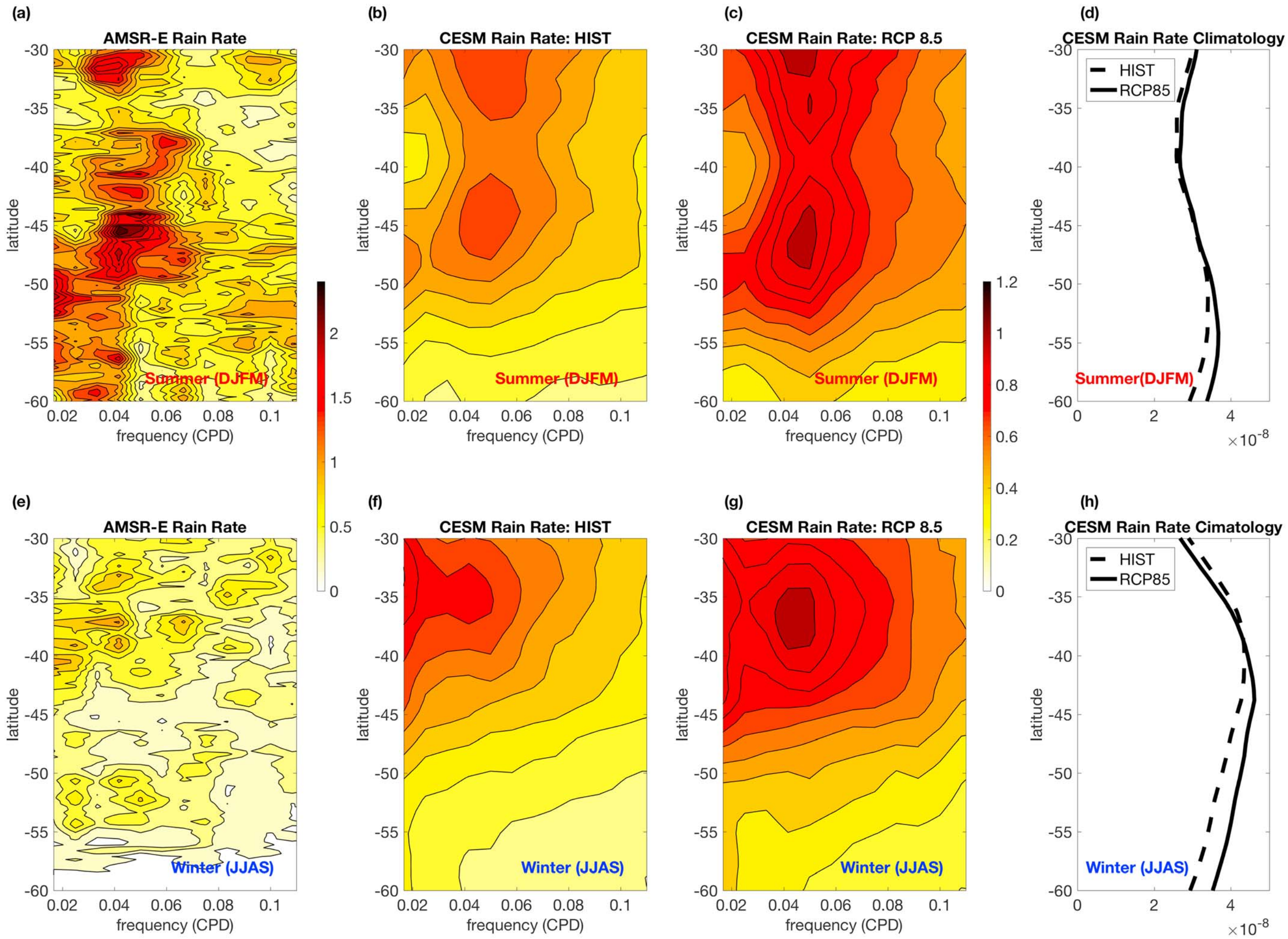

Figure 1. The robust increase of the precipitation intraseasonal variability in the Community Earth System Model (CESM) Large Ensemble simulations. (a and e) The power spectrum of satellite observed rain rate AMSR-E, (b and f) 40-member ensemble-mean rain rate from CESM Large Ensemble historical simulations (1975–2005), and (c and g) corresponding rain rate in the RCP 8.5 scenario (2070–2100). Note the different color bar range for the AMSR-E results and CESM results. (d and h) Ensemble-mean seasonal-mean zonal-mean rain rate from CESM Large Ensemble historical period (dashed) and RCP 8.5 period (solid). The upper panels show the austral summer (December–March), and the lower panels show austral winter (June–September). The power spectrum of rain rate has a unit of 10^{-16} m^2, and the rain rate has a unit of ms^{-1}.

Toward the end of the century, the peak latitude of the precipitation periodicity in SH summer not only shifts poleward by 2° but also strengthens significantly (Figures 1c and 1g). For SH winter, the currently weak 20–30 day periodicity around 34–44°S becomes more prominent at intraseasonal time scale compared with that of the current climate. Both seasons see a substantial increase of intraseasonal variability. This stands in stark contrast to the weak change of the seasonal-mean precipitation at the corresponding latitudes (Figures 1d and 1h).

3.3. A Robust Increase of Storm Track Activity in CESM Large Ensemble

As shown in Wang and Nakamura (2015), the 850-hPa eddy heat flux is the major driver of the density-weighted FAWA and thus is an integral component of the 20–30 day periodicity. This is confirmed in Figures 2a and 2b. The strength of the 20–30 day periodicity increases robustly in austral summer. Interestingly, the peak latitude of the 20–30 day periodicity in eddy heat flux does not show a discernible poleward shift, suggesting that the cyclone genesis of midlatitude cyclones does not move poleward with the zonal mean wind. In winter, a similar strengthening of midlatitude maximum of variance at intraseasonal time scale can be identified as well, although the BAM maximum itself is less dominant than the high eddy

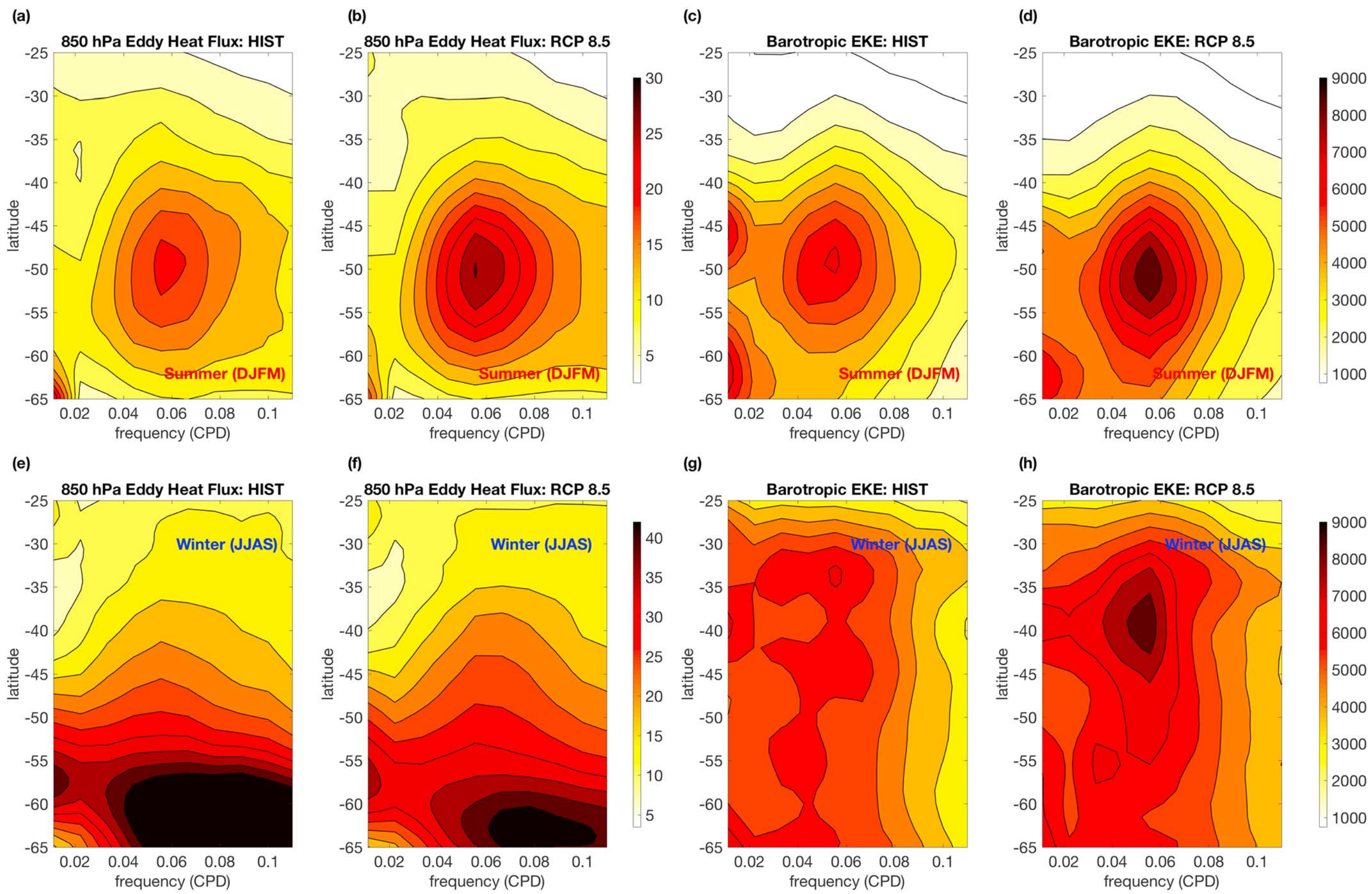

Figure 2. The robust increase of low-level eddy sensible heat flux and vertically averaged eddy kinetic energy (EKE) variability in the Community Earth System Model Large Ensemble simulations. Power spectra of the 850-hPa eddy heat flux in the (a and e) historical period and in the (b and f) RCP 8.5 period. Power spectrum of the density-weighted vertically averaged EKE in the (c and g) historical period and in the (d and h) RCP 8.5 period. The upper panels show the austral summer (December–March), and the lower panels show austral winter (June–September). The unit for eddy heat flux power spectrum is m^2K^2, and the unit for EKE power spectrum is $m^4 s^{-2}$.

heat flux at higher latitudes (i.e., 65 S), which is strongly affected by Antarctica's thermal contrast in winter. The relative small change in the low-level cyclone genesis is consistent with the notion that baroclinic eddies propagate longer distance poleward in a warming climate revealed by the Lagrangian tracking by Tamarin-Brodsky and Kaspi (2017). Thus, the poleward shift of EKE may be attributed to the more poleward propagation of baroclinic eddies instead of the change in cyclone genesis.

We next turn our attention to the storm track activity measured by the column-averaged EKE with the density weighting to avoid the influence due to the well-documented upward expansion of jet stream and transient eddies in a warming climate (Kushner et al., 2001; Lorenz & DeWeaver, 2007). In SH summer, we find that the variability of column-averaged EKE becomes much stronger, while the seasonal-mean EKE is primarily characterized by a poleward shift. Similar to the change in precipitation, in SH winter, the variability of EKE in the present climate will increase significantly between 34°S and 44°S. This pattern of the EKE variability change is consistent with that of the precipitation, except that the EKE variability change is extended further poleward. In short, in a warming climate, both summer and winter will feature a more robust 20–30 day periodicity of EKE respectively peaking at different latitudes.

While in summer the zonal-mean subtropical jet and eddy-driven jet merge at around 45°S, in winter the two jets tend to be separated meridionally. For both seasons, the peak latitudes of 20–30 day periodicity follow the location of the zonally coherent jets (in winter it is the subtropical jet and in summer it is the merged jet), as the latter provides favorable waveguides for Rossby wave interference and thus critical for the 20–30 day amplitude modulation (Wang & Nakamura, 2016). On top of that, the abundant water vapor around subtropical jets can release adequate diabatic heating, which may further fuel the propagating Rossby waves and the strength of the 20–30 day periodicity.

3.4. Fractional Change of the 20–30 Day Periodicity and the Seasonal-Mean Quantities

We next investigate whether the increased power spectrum is unique for the 20–30 day frequency range or it is ubiquitous for all other frequencies. The CESM LENS outputs have adequate spatial and temporal resolutions, which allow us to calculate the EKE at all vertical levels on daily resolution for all 40 ensemble members.

We calculate the fractional change between RCP 8.5 and historical simulations in the square root of the power spectrum within the BAM latitudes, that is, 46°S–56°S for austral summer and 34°S–44°S for austral winter according to the latitudinal extent of the 20–30 day periodicity in EKE. The square root of the power spectrum is adopted in order to be consistent with the dimension of the original quantity. Choosing a wider midlatitude average (30°S–60°S) yields similar results (see Figure S3 in the supporting information). For all variables, the fractional change represents the change over a time span of 95 years between 1976–2005 and 2071–2100.

In austral summer, a greater enhancement in the variability of rain rates, eddy heat fluxes, and EKE can be identified within the 20–30 day range in Figures 3a and 3b. Since the specific humidity scales with the temperature change via the Clausius-Clapeyron relation and both the mean temperature warming and the increase in the standard deviation of temperature contribute to the increase of moisture variability, we expect large enhancement in the eddy moisture flux. This indeed is evidenced by the 40% increase of the 850-hPa moisture flux (cyan) in the 20–30 day frequency range in Figure 3a. Among the 40%, only ~5% is from the enhancement of eddy meridional velocity at the 850 hPa given the approximate 10% enhancement of the EKE (Figure 3b). In addition, the percentage increase of eddy moisture flux is significantly higher than that of eddy sensible heat flux for both summer and winter (Figures 3a and 3b).

The rain rate has a marked enhancement of over 25% at the 20–30 day frequency range, stronger than the 19% enhancement in other frequency range. The column-averaged EKE is enhanced by about 20% at the 20–30 day frequency range, and no significant increase can be found in other higher frequency range. The consistent change unique to the 20–30 day frequency range suggests a plausible dynamical coupling between low-level moisture and tropospheric wave activity. While the detailed mechanism of this dynamical coupling will be left for future investigation, the basic idea is sketched below.

To the first order, the standard deviation of precipitation $\boldsymbol{P}$ scales with zonal-mean moisture content $\boldsymbol{q}$ and vertical eddy velocity $\boldsymbol{w}'$:

$$\boldsymbol{P} \sim \overline{\boldsymbol{q}}\sqrt{\overline{\boldsymbol{w}'^2}} \tag{1}$$

Assuming the aspect ratio of the circulation does not change in the midlatitudes, the dynamical contribution from changing vertical velocity w' can be inferred from the change of 850-hPa meridional eddy velocity standard deviation in Figure 3b, which is about 5%, leaving 20% to the increase of the moisture which scales well with the roughly 3 K near-surface temperature warming in these simulation (not shown).

In contrast to the 10% fractional change of 850-hPa meridional eddy velocity standard deviation, standard deviation in the column-averaged EKE sports a higher fractional change of 20%, which is primarily contributed by the upper troposphere where climatology EKE is stronger. This enhanced fractional change of column-averaged EKE suggests an enhanced dynamical coupling between lower and upper troposphere in the 20–30 day frequency range. In other frequencies in austral summer, the standard deviation of 850-hPa meridional eddy velocity (and presumably vertical velocity) is not significantly changed; therefore, the change of standard deviation of precipitation is predominantly due to the increased moisture content $\boldsymbol{q}$, whereas the 20–30 day precipitation standard deviation is further enhanced by the increasing vertical velocity.

The fractional change of variability in winter is different from that in summer. No clear enhancement unique at the 20–30 day frequency range can be identified. Instead, for both moisture flux and rain rate, the increase is rather homogeneous across different frequencies. The 850-hPa meridional eddy standard deviation and density-weighted EKE also increase similarly at all frequencies, which may be due to a

10.1029/2018GL078495

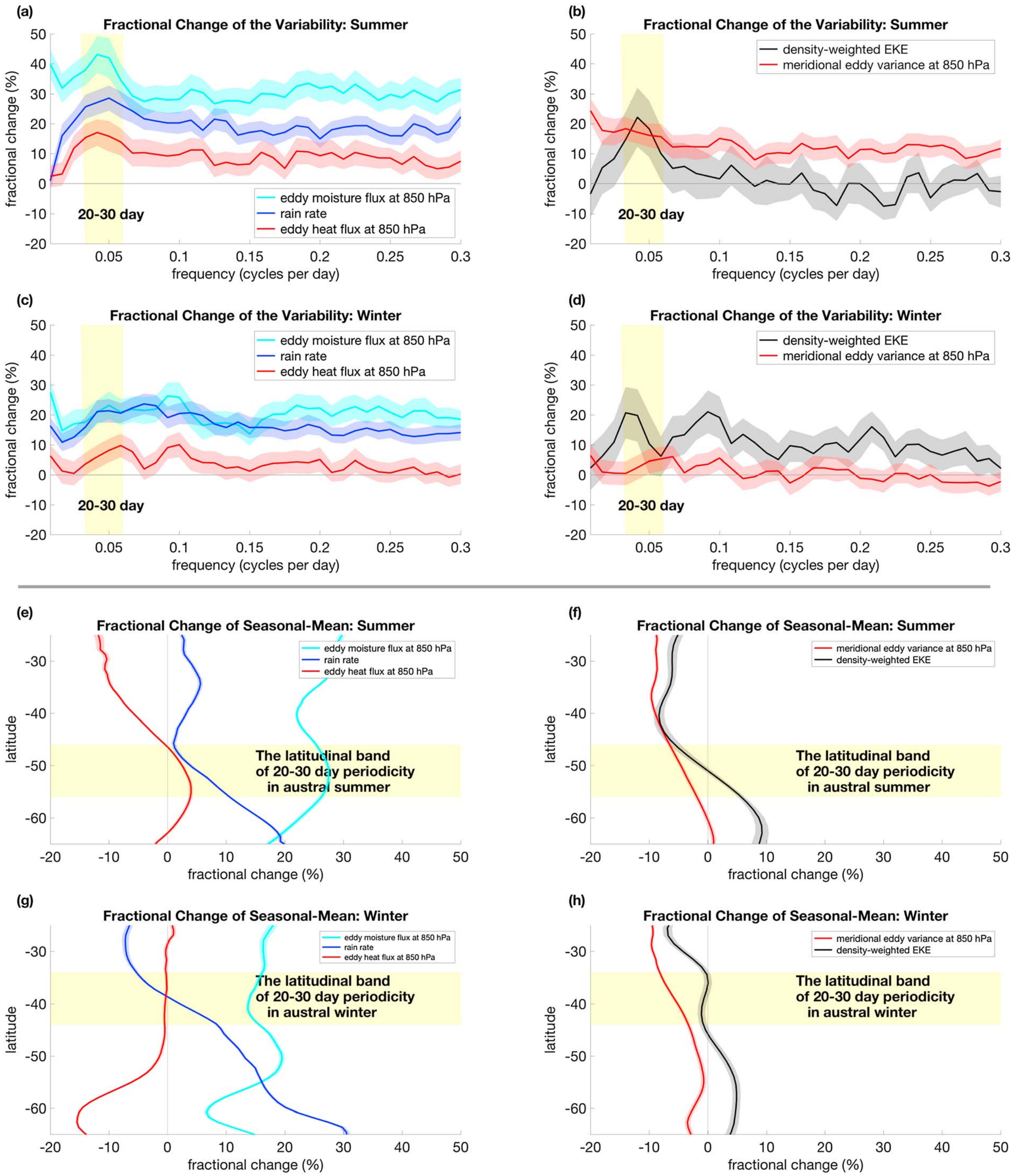

Figure 3. Fractional change of 850-hPa sensible and moist eddy fluxes, rain rate, meridional eddy velocity standard deviation, and density-weighted vertical average of eddy kinetic energy (EKE) in the Community Earth System Model Large Ensemble simulations. The upper two rows show the fractional change of the intraseasonal variability of the above quantities over the baroclinic annular mode latitudes (46°S–56°S in austral summer and 34°S–44°S in austral winter), while the lower two rows show the fractional change of the seasonal-mean quantities. In all panels, the probability density function (PDF) distribution of the fractional change is obtained using a kernel fitting for all 40 ensemble members. The curves are the maximum PDF, and the shading denotes the 95% confidence interval. (a and c) Fractional changes of the square root of the variance of 850-hPa eddy moisture flux (cyan) and eddy sensible flux (red), rain rate (blue). (b and d) Fractional change of the square root of the variance of 850-hPa meridional eddy velocity (red) and density-weighted EKE (black). In (a)–(d), all values are averaged between the 20–30 day periodicity latitudes defined in the text, and the 20–30 day frequency range is denoted by a yellow band. (e–h) The 20–30 day periodicity region defined in the text is denoted by a yellow band. The first and third rows show the austral summer (December–March), and the second and fourth rows show austral winter (June–September).

lack of dynamical organization from the strong waveguide effects as in the austral summer. Nevertheless, in terms of absolute change, in light of the elevated standard deviation at the 20–30 day frequency in the current climate, the standard deviation at the frequency range of 20–30 day will increase more than other frequencies. As a result, the 20–30 day variability will be more impactful for regulating large-amplitude wave events.

In Figures 3e–3h, we find that the fractional change of seasonal-mean quantities within the latitudinal band of the 20–30 day periodicity is substantially smaller than the change of the standard deviations, except for the eddy moisture flux, which again shows the strongest increase (albeit still slightly smaller than its fractional change in the intraseasonal variability). The seasonal-mean 850-hPa meridional eddy velocity standard deviation is reduced at all latitudes for both seasons, suggesting an overall reduced low-level kinematics in the storm tracks. With the increased moisture, eddies can transport moist static energy more efficiently and eddies are more organized around the 20–30 day frequency range as shown in Figures 3a and 3b. For eddy sensible heat fluxes, the seasonal-mean increases no more than 5% even at the peak latitude; it decreases for most of the latitudes (Figures 3e–3h). For seasonal-mean precipitation, the latitude of BAM sits right at the nodal point of the poleward shift, thus features the smallest fractional change in the mean precipitation compared with that in subtropics and higher latitudes. Interestingly, while the change of the intraseasonal variability of column EKE is characterized by an intensification by 20% at the latitudes of the 20–30 day periodicity, the seasonal-mean density-weighted EKE primarily exhibits a meridional dipole structure following the poleward shift of the jet, with little seasonal-mean change near the peak latitudes of BAM.

Regarding the horizontal structure of the fractional change, the column EKE variability increases preferentially at BAM latitudes for both seasons (see Figure S1). The vertical structure of the fractional change of the EKE variability demonstrates a vertical dipole structure: While EKE variability will decrease slightly in the lower troposphere, EKE variability will increase significantly near tropopause (~100 hPa). The reduction of the low-level EKE variability can be understood as baroclinic moist eddies becoming more efficient on transporting moist static energy poleward, thus requiring an overall smaller wave amplitude. Interestingly, for both SH summer and winter, the 20–30 day frequency range features a vertically coherent increase of EKE variability throughout the troposphere.

According to the definition of the predictability based on the information theory (e.g., DelSole & Tippett, 2007), it is the sharpness, not the location, of the spectral peak of a damped oscillator like BAM that evinces the predictability. The more prominent peaks at the 20–30 day frequency range of BAM seen in the future warming scenario imply that BAM will become even more predictable as climate warms.

3.5. A Consistent Increase of Intraseasonal Variability in the CMIP5

To verify the robustness of the increase of the BAM variability detected from the CESM LENS, we further show that qualitatively similar behavior can be found in other climate models in the CMIP5 (Taylor et al., 2012; see Figures S4–S7). Daily precipitation, daily meridional wind and air temperature at 850 hPa, and EKE at all 8 available levels from 20 selected models of the CMIP5 are used to compute the power spectra of precipitation, eddy heat flux, and EKE. The selection is to eliminate models with unreasonable biases in the climatological mean jet and mean eddy heat flux (see Text S1 in the supporting information). The same historical and RCP8.5 periods as the CESM LENS are used for the purpose of consistency. As different climate models feature different zonal-mean basic states, we calculate the fractional change in the spectral space based on the domain average between 30°S and 60°S.

We primarily focus on three variables—rain rates, 850-hPa eddy heat flux, and EKE. In Figures S4–S7, the fractional changes of the three variables prove to be in general consistent with what has been seen in CESM LENS, although, given that CMIP5 models with different basic states would place the 20–30 day power peak at different latitudes, the uncertainty range is substantially larger compared to CESM LENS.

Several salient features can be nevertheless identified from the CMIP5 analysis, which are consistent with the CESM LENS outputs: First, the intraseasonal variability of precipitation increases much more than the change of seasonal-mean change. Second, the 20–30 day standard deviation of 850-hPa eddy sensible flux gets preferentially increased in SH summer. Third, the standard deviation of 100-hPa EKE (and to a lesser extent the column-averaged EKE, which was calculated only based on the available 8 levels) gets enhanced at the intraseasonal time scales. Third, SH winter has a more uniform enhancement at all frequencies for precipitation and EKE.

4. Conclusions

This work examines the change of the intraseasonal variability in the SH storm track. The main results include the following:

1. We find a preferential intensification of the EKE and precipitation variability at intraseasonal time scale in the SH storm track in the RCP 8.5 scenario, compared to their corresponding seasonal-mean changes.
2. We highlight the fractional change is further enhanced in the 20–30 day frequency range, especially for SH summer, implicative of a more predictable BAM in a warmer climate.

While the fundamental dynamics of the 20–30 day periodicity are still under investigation, we have demonstrated that in climate model projections, the 20–30 day periodicity becomes an even more robust feature in a warming climate in both seasons. Toward the end of the century, the BAM not only shifts poleward by 2° as the jet shifts, but more importantly, the intensity of BAM increases significantly by 20% and 25% respectively for EKE and precipitation.

Our understanding of the origin of the 20–30 day periodicity of BAM is the constructive and destructive interference of Rossby waves within the waveguide of the zonally symmetric jet structure during austral summer (Wang & Nakamura, 2016). In a warming climate, a well-recognized feature is the narrowing and strengthening of the zonal jet, hence a stronger waveguide. This feature can be further evidenced by a robust enhancement of the low-level temperature gradient at BAM latitudes (see Figure S2) and linked to the robust enhancement of the SST gradient near the latitudes of storm track (e.g., Bengtsson et al., 2006; Marshall et al., 2015). This morphological change in the zonal wind and the associated waveguide effect may provide a dry-dynamics basis for the enhancement of the 20–30 day variability.

More importantly, a distinct attribute of the BAM from the annular mode is that it can be directly driven by a diabatic wave source (Wang & Nakamura, 2016), while annular mode is only directly driven by eddy momentum flux convergence and damped indirectly by the diabatic processes (Xia & Chang, 2014). The BAM occurs primarily near the subtropical jet in winter and more in alignment with the merged jet in summer, both of which featuring abundance of moisture for diabatic heating. Thus, an increased diabatic heating in a warming climate can cast impact directly on the 20–30 day periodicity by providing additional diabatic PV sources to energize Rossby waves.

In recognition of the involvement of both the dry and moist processes in the BAM variability, we speculate that the enhanced waveguide effect provides a favorable environment for wave packet interference and the increasing moisture supports a stronger diabatic feedback for the intraseasonal variability of the BAM. Further mechanistic inquiries using a hierarchy of models and purposely designed experiments are needed to unravel the root cause for the enhancement of the intraseasonal variability under climate warming.

Acknowledgments
The authors acknowledge the computational resources at NCAR Yellowstone and Harvard Odyssey cluster. The authors also acknowledge the World Climate Research Programme's Working Group on Coupled Modeling, which is responsible for CMIP, and we thank the climate modeling groups for producing and making available their model output. This research was supported by NASA grant 80NSSC17K0267, NSF grant AGS-1552385, and a grant from the Harvard Global Institute. J.L. was supported by the U.S. Department of Energy Office of Science Biological and Environmental Research (BER) as part of the Regional and Global Climate Modeling program. AMSR data are produced by Remote Sensing Systems and were sponsored by the NASA AMSR-E Science Team and the NASA Earth Science MEaSUREs Program. Data are available at www.remss.com. The CMIP5 data used in this study are freely available through the Earth System Grid Federation (https://esgf-node.llnl.gov).

References

Ahmadi-Givi, F., Graig, G. C., & Plant, R. S. (2004). The dynamics of a midlatitude cyclone with very strong latent-heat release. *Quarterly Journal of the Royal Meteorological Society*, *130*(596), 295–323. https://doi.org/10.1256/qj.02.226

Barnes, E. A., & Polvani, L. (2013). Response of the midlatitude jets, and of their variability, to increased greenhouse gases in the CMIP5 models. *Journal of Climate*, *26*(18), 7117–7135. https://doi.org/10.1175/JCLI-D-12-00536.1

Bengtsson, L., Hodges, K. I., & Roeckner, E. (2006). Storm tracks and climate change. *Journal of Climate*, *19*(15), 3518–3543. https://doi.org/10.1175/JCLI3815.1

Chang, E. K. M., Guo, Y., & Xia, X. (2012). CMIP5 multimodel ensemble projection of storm track change under global warming. *Journal of Geophysical Research*, *117*, D23118. https://doi.org/10.1029/2012JD018578

DelSole, T., & Tippett, M. K. (2007). Predictability: Recent insights from information theory. *Reviews of Geophysics*, *45*, RG4002. https://doi.org/10.1029/2006RG000202

Grise, K. M., & Polvani, L. M. (2014). The response of midlatitude jets to increased CO_2: Distinguishing the roles of sea surface temperature and direct radiative forcing. *Geophysical Research Letters*, *41*, 6863–6871. https://doi.org/10.1002/2014GL061638

Guan, B., & Waliser, D. (2017). Extreme winds and precipitation during landfall of atmospheric rivers. *Nature Geoscience*, *10*(3), 179–183. https://doi.org/10.1038/ngeo2894

Hall, N. M. J., Hoskins, B. J., Valdes, P. J., & Senior, C. A. (1994). Storm tracks in a high-resolution GCM with doubled carbon dioxide. *Quarterly Journal of the Royal Meteorological Society*, *120*(519), 1209–1230. https://doi.org/10.1002/qj.49712051905

Held, I. M., & Soden, B. J. (2006). Robust responses of the hydrological cycle to global warming. *Journal of Climate*, *19*(21), 5686–5699. https://doi.org/10.1175/JCLI3990.1

Hoskins, B. J., McIntyre, M. E., & Robertson, A. W. (1985). On the use and significance of isentropic potential vorticity maps. *Quarterly Journal of the Royal Meteorological Society*, *111*(470), 877–946. https://doi.org/10.1002/qj.49711147002

Kay, J. E., Deser, C., Phillips, A., Mai, A., Hannay, C., Strand, G., et al. (2015). The Community Earth System Model (CESM) large ensemble project: A community resource for studying climate change in the presence of internal climate variability. *Bulletin of the American Meteorological Society*, *96*(8), 1333–1349. https://doi.org/10.1175/BAMS-D-13-00255.1

Kushner, P. J., Held, I. M., & Delworth, T. L. (2001). Southern hemisphere atmospheric circulation response to global warming. *Journal of Climate*, *14*(10), 2238–2249. https://doi.org/10.1175/1520-0442(2001)014<0001:SHACRT>2.0.CO;2

Lee, S., & Feldstein, S. B. (2013). Detecting ozone- and greenhouse gas-driven wind trends with observational data. *Science*, *339*(6119), 563–567. https://doi.org/10.1126/science.1225154

Lorenz, D. J., & DeWeaver, E. T. (2007). Tropopause height and zonal wind response to global warming in the IPCC scenario integrations. *Journal of Geophysical Research*, *112*, D10119. https://doi.org/10.1029/2006JD008087

Lu, J., Sun, L., Wu, Y., & Chen, G. (2014). The role of subtropical irreversible PV mixing in the zonal mean circulation response to global warming-like thermal forcing. *Journal of Climate*, *27*(6), 2297–2316. https://doi.org/10.1175/JCLI-D-13-00372.1

Marshall, J., Scott, J. R., Armour, K. C., Campin, J.-M., Kelley, M., & Romanou, A. (2015). The ocean's role in the transient response of climate to abrupt greenhouse gas forcing. *Climate Dynamics*, *44*(7–8), 2287–2299. https://doi.org/10.1007/s00382-014-2308-0

Nie, Y., Zhang, Y., Chen, G., & Yang, X.-Q. (2015). Delineating the barotropic and baroclinic mechanisms in the midlatitude eddy-driven jet response to lower-tropospheric thermal forcing. *Journal of the Atmospheric Sciences*, *73*(1), 429–448. https://doi.org/10.1175/JAS-D-15-0090.1

O'Gorman, P. A. (2010). Understanding the varied response of the extratropical storm tracks to climate change. *Proceedings of the National Academy of Sciences of the United States of America*, *107*(45), 19,176–19,180. https://doi.org/10.1073/pnas.1011547107

O'Gorman, P. A., & Schneider, T. (2009). The physical basis for increases in precipitation extremes in simulations of 21st-century climate change. *Proceedings of the National Academy of Sciences of the United States of America*, *106*(35), 14,773–14,777. https://doi.org/10.1073/pnas.0907610106

Pan, Y., Li, L., Jiang, X., Li, G., Zhang, W., Wang, X., & Ingersoll, A. P. (2017). Earth's changing global atmospheric energy cycle in response to climate change. *Nature Communications*, *8*. https://doi.org/10.1038/ncomms14367

Pendergrass, A. G., & Gerber, E. P. (2016). The rain is askew: Two idealized models relating vertical velocity and precipitation distributions in a warming world. *Journal of Climate*, *29*(18), 6445–6462. https://doi.org/10.1175/JCLI-D-16-0097.1

Singh, M. S., Kuang, Z., Maloney, E. D., Hannah, W. M., & Wolding, B. O. (2017). Increasing potential for intense tropical and subtropical thunderstorms under global warming. *Proceedings of the National Academy of Sciences of the United States of America*, *114*(44), 11,657–11,662. https://doi.org/10.1073/pnas.1707603114

Tamarin-Brodsky, T., & Kaspi, Y. (2017). Enhanced poleward propagation of storms under climate change. *Nature Geoscience*, *10*(12), 908–913. https://doi.org/10.1038/s41561-017-0001-8

Taylor, K. E., Stouffer, R. J., & Meehl, G. A. (2012). An overview of CMIP5 and the experiment design. *Bulletin of the American Meteorological Society*, *93*(4), 485–498. https://doi.org/10.1175/BAMS-D-11-00094.1

Thompson, D. W. J., & Barnes, E. A. (2014). Periodic variability in the large-scale southern hemisphere atmospheric circulation. *Science*, *343*(6171), 641–645. https://doi.org/10.1126/science.1247660

Thompson, D. W. J., Barnes, E. A., Deser, C., Foust, W. E., & Phillips, A. S. (2015). Quantifying the role of internal climate variability in future climate trends. *Journal of Climate*, *28*(16), 6443–6456. https://doi.org/10.1175/JCLI-D-14-00830.1

Thompson, D. W. J., & Woodworth, J. D. (2014). Barotropic and baroclinic annular variability in the Southern Hemisphere. *Journal of the Atmospheric Sciences*, *71*(4), 1480–1493. https://doi.org/10.1175/JAS-D-13-0185.1

Wang, L. (2016). Periodic behavior of finite-amplitude wave activity in the Southern Hemisphere storm track (Ph.D.). The University of Chicago, United States -- Illinois. Retrieved from https://search.proquest.com/docview/1864781969

Wang, L., & Lee, S. (2016). The role of eddy diffusivity on poleward jet shift. *Journal of the Atmospheric Sciences*, *73*(12), 4945–4958. https://doi.org/10.1175/JAS-D-16-0082.1

Wang, L., & Nakamura, N. (2015). Covariation of finite-amplitude wave activity and the zonal mean flow in the midlatitude troposphere. Part 1: Theory and application to the Southern Hemisphere summer. *Geophysical Research Letters*, *42*, 8192–8200. https://doi.org/10.1002/2015GL065830

Wang, L., & Nakamura, N. (2016). Covariation of finite-amplitude wave activity and the zonal mean flow in the mid-latitude troposphere. Part 2: Eddy forcing spectra and the periodic behavior in the Southern Hemisphere summer. *Journal of the Atmospheric Sciences*, *73*(12), 4731–4752. https://doi.org/10.1175/JAS-D-16-0091.1

Wentz, F. J., Meissner, T., Gentemann, C. L., & Brewer, M. (2014). Remote sensing systems AQUA AMSR-E daily and 3-day environmental suite on 0.25 deg grid, Version 7.0. Remote Sensing Systems, Santa Rosa, CA. https://doi.org/Availableonlineatwww.remss.com/missions/amsre.[Accessed 01 08 2016].

Xia, X., & Chang, E. K. M. (2014). Diabatic damping of zonal index variations. *Journal of the Atmospheric Sciences*, *71*(8), 3090–3105. https://doi.org/10.1175/JAS-D-13-0292.1

Yin, J. H. (2005). A consistent poleward shift of the storm tracks in simulations of 21st century climate. *Geophysical Research Letters*, *32*, L18701. https://doi.org/10.1029/2005GL023684

Zurita-Gotor, P. (2017). Low-frequency suppression of Southern Hemisphere tropospheric eddy heat flux. *Geophysical Research Letters*, *44*, 2007–2015. https://doi.org/10.1002/2016GL072247